Eur. Phys. J. A **27**, s01, 187–192 (2006)
DOI: 10.1140/epja/i2006-08-028-3

EPJ A direct
electronic only

Evidence for a host-material dependence of the n/p branching ratio of low-energy d+d reactions within metallic environments

A. Huke[1,a], K. Czerski[1,2], T. Dorsch[1], A. Biller[1], P. Heide[1], and G. Ruprecht[1,3]

[1] Institut für Atomare Physik und Fachdidaktik, Technische Universität Berlin, Hardenbergstr. 36, 10623 Berlin, Germany
[2] Institute of Physics, University of Szczecin, Szczecin, Poland
[3] TRIUMF, Vancouver, Canada

Received: 6 July 2005 /
Published online: 16 March 2006 –

Abstract. Angular distributions and the neutron-proton branching ratio of the mirror reactions ^{2}H(d, p)^{3}H and ^{2}H(d, n)^{3}He have been investigated using different self-implanted deuterized metallic targets at projectile energies between 5 and 60 keV. Whereas the experimental results obtained for the transition metals Zr, Pd, Ta and also Al do not differ from those known from gas-target experiments, an enhancement of the angular anisotropy in the neutron channel and an attenuation of the neutron-proton branching ratio have been observed for the (earth)alkaline metals Li, Sr and Na at deuteron energies below 20 keV. Experimental results are discussed with consideration of the special problems arising from the properties of these chemically very reactive target materials. A first theoretical effort explaining simultaneously both n/p asymmetry effects based on an induced polarization of the reacting deuterons within the crystal lattice is presented.

PACS. 24.70.+s Polarization phenomena in reactions – 25.45.Hi Transfer reactions – 26.20.+f Hydrostatic stellar nucleosynthesis – 89.30.Jj Nuclear fusion power

1 Introduction

The d+d reactions have been investigated for decades because of their simplicity, fundamental importance and possible application in energy generation technology (*e.g.*, see the compilation [1]). Two of the three exit channels ^{2}H(d, p)^{3}H and ^{2}H(d, n)^{3}He generating high energetic particles are mediated by the strong interaction with a branching ratio of about 1 below 50 keV while the third one ^{2}H(d, γ)^{4}He is an electromagnetic transition suppressed by $> 10^7$. Close to the reaction threshold there are two 1^- resonances in the compound nucleus ^{4}He. They can be excited by deuterons with an orbital angular momentum of 1. For this reason the extraordinary strong anisotropy of the angular distribution of the ejectiles even at the lowest energies can be observed. These facts are well known mostly from experiments on gas and polyethylene targets.

There is multiple evidence that the physical environment where the nucleus is embedded can influence nuclear interactions, *e.g.* this is employed in nuclear condensed matter physics. Also in astrophysics the prolongation of the life period of ^{7}Be in the stellar plasma plays an important role in the solar model, *e.g.* [2] and references therein.

[a] e-mail: huke@physik.tu-berlin.de

In order to investigate the environmental impact on nuclear reactions, we experiment with the d+d reactions in metallic environments. We have already found a strongly enhanced electron screening effect leading to a gross increase of the effective cross section by abatement of the Coulomb barrier due to the metal electrons [3,4] which was later reconfirmed [5]. Angular distributions and relative intensities of the proton and neutron channels investigated for d+d reactions taking place in Al, Zr, Pd and Ta targets were, however, in agreement with the results of gas-target experiments. Here we present new results obtained for Sr, Li and Na targets giving a first evidence for an alteration of the neutron-proton branching ratio and the angular distributions. The experiment was published in [6,7] and now a first theoretical explanation for this surprising observation can be presented [8,9].

2 Experimental results

The experiment has been carried out at an electrostatic cascade accelerator at beam energies below 60 keV maintained by a highly stabilized power supply. The deuterium beam ions were generated by an RF ion source with final currents at the target $< 200\,\mu$A depending on the energy. The principal set-up of the detection facility is outlined

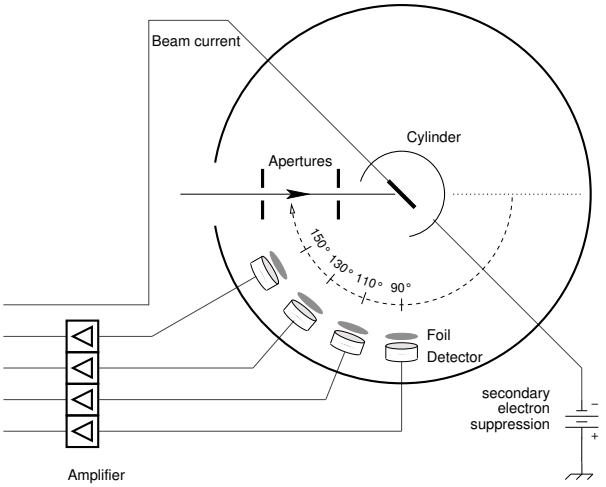

Fig. 1. The set-up in the target chamber.

in fig. 1. After having traversed electrostatic quadrupoles and magnetic dipoles the beam is finally formed by two apertures with a diameter of 1 cm. The targets were pure metal disks becoming self-implanted deuterium targets under the deuteron irradiation. Four Si-detectors with an active surface diameter of 1 cm at a distance of 10 cm and the laboratory angles of 90°, 110°, 130° and 150° were used for the detection of all charged particles, p, t, ^{3}He, of the reactions ^{2}H(d, p)t and ^{2}H(d, n)^{3}He [4]. The detectors needed to be shielded from the backscattered deuterons in order to prevent a congestion of them and the data acquisition system. Therefore grounded Al foils of thicknesses from 120–150 μg/cm^2 were placed in front of the detectors insulated from them. The thickness is sufficient in order to stop backscattered deuterons up to 60 keV. The solid angles surveyed by the detectors were determined with a radioactive α source.

The low-energy part of some representative spectra from the 90° detector is depicted in fig. 2 magnifying the two lines of the recoil nuclei ^{3}He and t. The integral counting number of the spectra are normalized to unity in order to make them comparable. The energies above the peaks are the kinetic energies of the ejectiles in the laboratory system. They drop for increasing projectile energies, which is especially significant for the back angle positions. The gray filled spectra are from Ta targets, while the black and gray step lines are for Sr and Li and Na, respectively. The two plots compare the form of the spectral lines at a low projectile energy of 8 keV to a high energy of 30 keV. At 8 keV the t-line of Ta is well separated while the ^{3}He-line sits on an exponential background. The background is subtracted by fitting an exponential function to the lowest energy part and then by extrapolating it to the high energies. The spectral lines for Sr are already broader with an enhanced low-energy tail leading to an overlap of both lines. This effect becomes even stronger for Li and Na. At 30 keV the Ta lines are broader but the tails of the Sr, Li and Na lines are much more distinctive. The overlap of the two lines is even higher. For Li and Na the ^{3}He-line is hardly more than an edge. The p-line at 3 MeV has

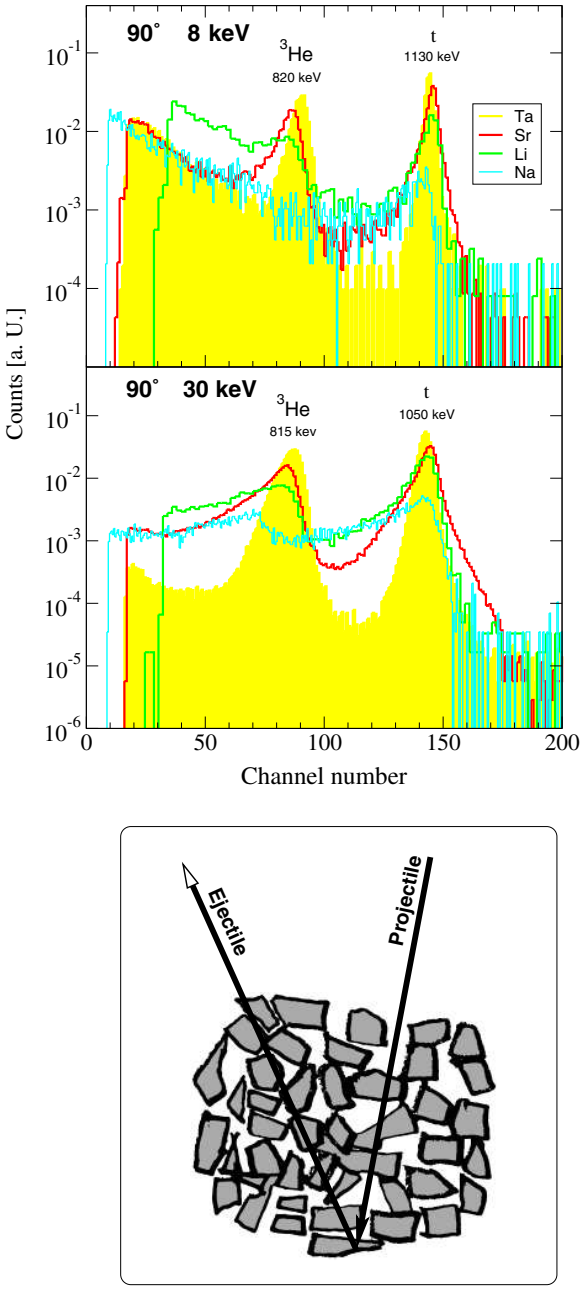

Fig. 2. Normalized spectra from the 90° detector obtained at deuteron energies 8 and 30 keV. The low-energy tail complicates the discrimination and is caused by embrittlement which becomes stronger for more reactive metals. The sketch shows how different paths through the target explain the tails.

also a long low-energy tail but it vanishes before the t-line. The appearance and the properties of these tails can be explained by a phenomenon known from the physical chemistry of the metal hydrides, called *embrittlement* [10] which means that the crystal structure of the metal is bursted by the recrystallization process that accompanies the formation of the metal hydride crystal. Reactive metals change their crystal structure while forming the metal

hydride. If the hydration precedes not in a thermal equilibrium and relatively slowly, the material cannot compensate the tension of the recrystallization process and bursts. Since deuteron implantation is far off the thermal equilibrium, embrittlement is a hardly avoidable concomitant phenomenon for reactive metals. How embrittlement effectuates the tails is elucidated with the sketch in fig. 2. Assuming the projectile travels through the target along a path covering many empty regions, the energy loss becomes smaller and consequently the nuclear reactions occur deeper below the target surface than in the case of compact materials. Therefore the ejectiles that in turn can travel through more compact target regions loose more energy additionally contributing to the low-energy tail of the particle spectrum. The increase of the tail with the projectile energy arises from the simultaneous increase in the range of the projectiles. The material dependence can be explained, too. Ta is almost a noble metal with low reactivity but nonetheless able to chemically bind hydrogen to high amounts. It just stretches its lattice but does not recrystallize like the highly reactive metals of the groups I and II of the periodic system. So there is no embrittlement and hardly a tail visible. On the other hand, the effects of embrittlement and the tail increase from Sr over Li to Na with decreasing electron negativity. The symptoms were even visible, *e.g.* dust particles crumbled from a strontium target, the thickness of a sodium target grew considerably. The low-energy tail formation complicates the integration of the spectral lines till infeasibility in the case of Na. The ^{3}He-line sits on the tail of the t-line. All efforts to describe and extrapolate the tail of the t-line to the lower energies analytically failed, since the form of the lines is dependent on the nucleus species, ejectile and projectile energy. Uncertainties in the integral of the spectral lines are taken into account in the errors additionally to the counting statistic. Consequently they are the dominating error source. If in doubt, counts were attributed to the ^{3}He-line only, gaining a conservative estimate of the n/p branching ratio at least. Fortunately, the tails are small at the low projectile energies where the asymmetry in the branching ratios becomes observable. The problems of integrating the overlapping spectral lines cannot be circumvented by the use of detector telescopes for particle identification. The ΔE-detector of the usual semiconductor detector telescopes would already absorb the recoil nuclei.

Another problem affecting the results comes from a property of RF ion sources inherent to their design. The extraction of the ions from the plasma within the source is done with an electric field which is formed by an extraction channel made from pure aluminium inside a ceramic cylinder. This extraction channel presets the direction, focus and flux profile of the beam prior to the lenses in front of the acceleration line. Because of its contact to the plasma and its small dimensions in order to throttle the gas loss it is a wear out commodity. The burn down proceeds not necessarily symmetrical relative to the geometrical axis. Thus, the beam direction and flux profile can gradually change during the wear out causing a shift of the flux distribution within the beam spot on the target.

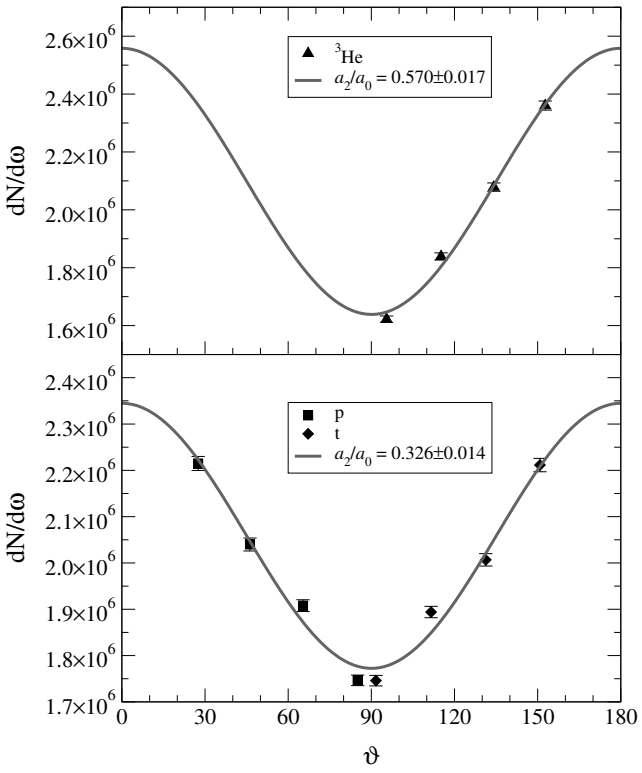

Fig. 3. Angular distribution of the ^{2}H(d, p)^{3}H and ^{2}H(d, n)^{3}He reactions obtained at the deuteron energy $E_d = 20\,\mathrm{keV}$ for Sr.

If this shift occurs within the plain stretched by the detectors and the target, the relative counting number among the detectors is altered leading to a likewise distortion of the angular distribution. Here a close detector geometry was set up facing a large beam spot, thus aggravating the problem. On the other hand a set-up in far geometry with a small beam spot would suffer from low counting rates.

Neglecting $l \geq 2$ contributions, the angular distribution can be described as follows:

$$\frac{\mathrm{d}\sigma}{\mathrm{d}\omega}(\vartheta) = A_0 + A_2 \cos^2\vartheta\,. \tag{1}$$

Because of the identical bosons in the entrance channel the angular distribution is symmetric around 90°. ϑ and ω are the polar angle and the solid angle in the CM system, respectively. Since the experimentally determined thick target yield for reactions far below the Coulomb barrier is dominated by the high energy contributions a similar expression is valid for the differential counting number

$$\frac{\mathrm{d}N}{\mathrm{d}\omega}(\vartheta) = a_0 + a_2 \cos^2\vartheta\,. \tag{2}$$

The expansion coefficients a_0 and a_2 now include constant factors describing detector and target properties and the number of incident projectiles. Consequently, the anisotropy coefficient can be defined as $\frac{a_2}{a_0} \approx \frac{A_2}{A_0}$. A measurement at 20 keV for Sr exemplary shows the results

Table 1. Anisotropy and branching ratios tabulated over the deuteron energy in keV in the laboratory system.

E_d^{lab}	$\frac{a_2}{a_0}$ (^{3}He)	$\frac{a_2}{a_0}$ (p)	$\frac{\sigma_n}{\sigma_p}$
Ta			
8.01	0.33±0.04	0.22±0.04	1.007±0.015
10.01	0.42±0.02	0.225±0.019	0.995±0.007
12.02	0.430±0.017	0.210±0.015	0.990±0.005
14.02	0.459±0.019	0.227±0.016	0.998±0.006
17.08	0.492±0.016	0.226±0.014	0.996±0.005
25.05	0.504±0.005	0.251±0.004	1.0030±0.0014
30.02	0.538±0.007	0.281±0.006	1.013±0.002
35.02	0.553±0.007	0.288±0.006	1.017±0.002
40.03	0.582±0.006	0.300±0.005	1.0187±0.0019
45.02	0.633±0.006	0.357±0.005	1.0209±0.0018
50.02	0.692±0.006	0.384±0.005	1.0230±0.0017
Sr			
7.01	0.49±0.05	0.20±0.04	0.837±0.013
8.01	0.54±0.02	0.208±0.016	0.909±0.006
10.01	0.458±0.018	0.245±0.015	0.948±0.006
12.02	0.455±0.012	0.194±0.010	0.923±0.004
14.02	0.372±0.015	0.182±0.013	0.991±0.006
17.02	0.440±0.012	0.214±0.010	0.971±0.004
20.02	0.473±0.014	0.283±0.012	0.991±0.005
25.04	0.506±0.013	0.247±0.011	0.992±0.004
30.04	0.505±0.015	0.286±0.005	1.025±0.003
35.19	0.587±0.007	0.274±0.005	1.021±0.002
40.02	0.669±0.007	0.369±0.004	1.0356±0.0019
45.03	0.550±0.004	0.269±0.003	1.0361±0.0014
50.03	0.640±0.005	0.334±0.004	1.0295±0.0015
55.02	0.684±0.005	0.327±0.004	1.0478±0.0014
Li			
8.02	1.9±1.9	0.25±0.06	0.83±0.19
10.02	0.9±0.3	0.30±0.03	0.79±0.05
12.02	0.9±0.3	0.41±0.03	0.77±0.04
14.03	1.3±0.3	0.66±0.03	0.85±0.05
17.02	0.59±0.14	0.304±0.011	1.02±0.04
25.01	0.96±0.19	0.39±0.04	0.98±0.04

for the differential counting number and the corresponding fitting function in fig. 3. The fit is computed with a non-iterative generalized linear fitting algorithm employing singular value decomposition thus allowing for more accurate values and better error handling. The data points obtained for the protons are included. As can be seen protons and tritons follow the same angular distribution. One observes a significantly stronger angular anisotropy for the neutron channel. Due to the strong energy dependence of the reaction cross sections, the branching ratio of the two mirror reactions can be obtained by dividing the thick target yields Y and correspondingly the total counting numbers N:

$$\frac{\sigma_{d(d,n)^3He}}{\sigma_{d(d,p)t}} \approx \frac{Y\left(^3\mathrm{He}\right)}{Y(\mathrm{p})} = \frac{N\left(^3\mathrm{He}\right)}{N(\mathrm{p})} = \frac{a_0\left(^3\mathrm{He}\right) + \frac{1}{3}a_2\left(^3\mathrm{He}\right)}{a_0(\mathrm{p}) + \frac{1}{3}a_2(\mathrm{p})}. \quad (3)$$

When calculating with the fitting coefficients one must consider that they are not independent variables. Then the Gaussian error propagation formula needs to be completed by a term containing the off-diagonal element of the covariance matrix from the fit.

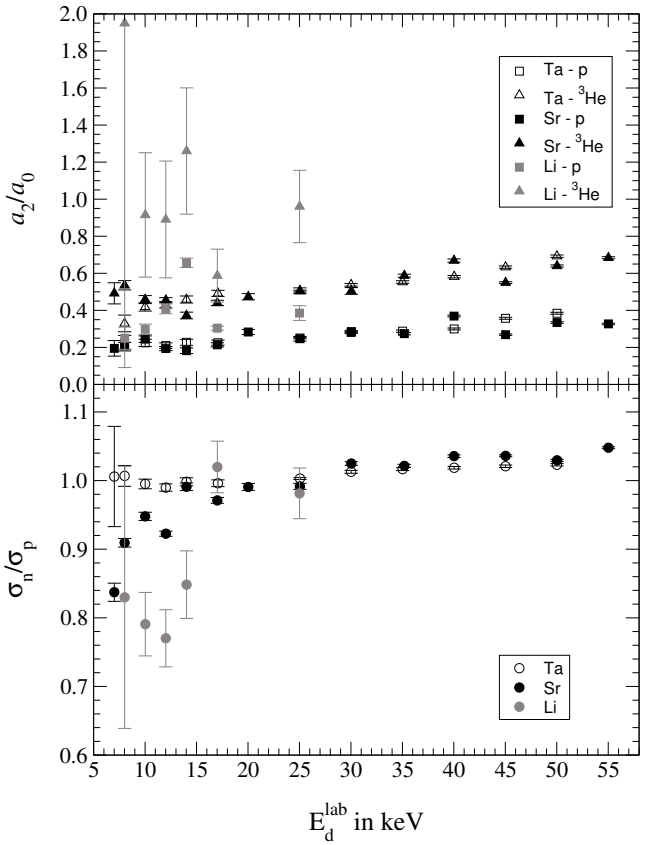

Fig. 4. The upper part displays the anisotropy from the detection of the p and ^{3}He ejectiles. The lower part shows the branching ratio of the two mirror reactions.

The results are listed in table 1 and plotted in fig. 4. The branching ratios and angular distributions for Ta agree with the results of the gas target experiment [11] and due to the much higher target nuclei density the data set has a notedly higher precision and extends to lower energies ([4], fig. 1). This agreement applies likewise to Al, Zr and Pd. Not so for Sr and Li. While for p there are no peculiarities, for ^{3}He the anisotropy raises at lower energies. Simultaneously, the n branch is suppressed. This is better cognizable in the rescaled fig. 5 for Sr. The results for protons and tritons are concordant. The low quality of the Li points results from the ambiguity of the integration of the spectral lines with large low-energy tails. For the same reason, the spectra obtained for Na could not be analyzed quantitatively, though the spectra indicate a strong suppression of the neutron-proton ratio at low energies, too. Because of the relative alteration in the counting numbers of the detectors from the burn down of the extraction channel the angular anisotropies obtain a gradually increasing positive offset corresponding to the sequence of the measurement campaign. Starting with Ta the value of the offset increased for Sr, Li, Zr and finally culminated at Al. Therefore the anisotropy data for Sr in table 1 and figs. 4, 5 was renormalized to the ones of Ta. Note: the anisotropy values in fig. 3 are the original ones. These corrections, however, hardly affect the branching

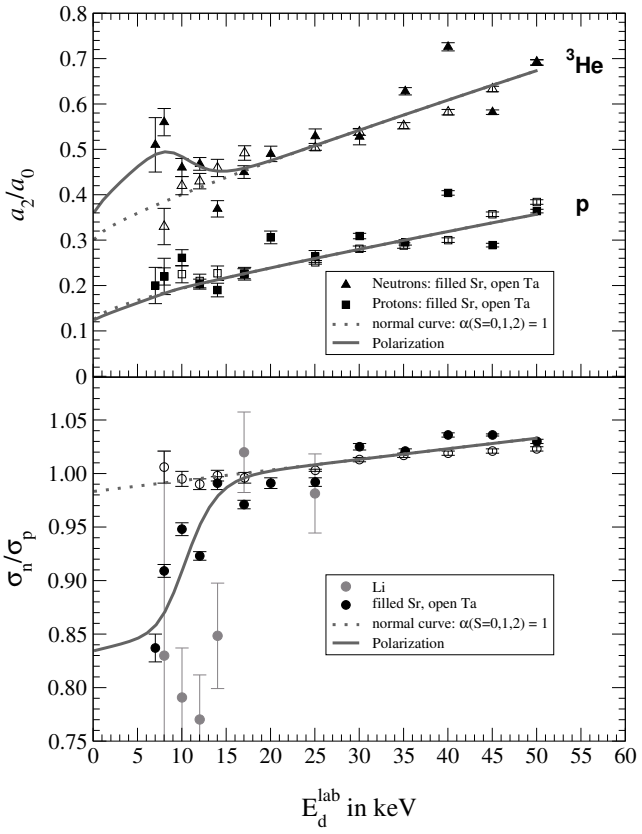

Fig. 5. The dashed line represents the normal curve. The solid lines result from a deuteron polarization corresponding to a suppression of the $S = 0$ channel at lower energies.

ratios (3). From the anisotropy presented in fig. 5 it can be seen that there are significant deviations from the smooth progression of the curve at 40 and 45 keV. They originate from suboptimal beam focus adjustment with accordingly beam flux shifts because of necessary beam current reductions at higher deuteron energies. The deviations occur likewise for protons and ^{3}He. Altogether an additional systematic error is introduced. For details refer to [6].

3 Theoretical considerations and discussion

Multiple scattering of the ejectiles in the thick target could possibly redirect leaving particles depending on the nucleus species and thereby change the detection rate. In order to test this, a Monte Carlo simulation was performed tracing the path of the reaction ejectiles [12]. The target bulk is assumed to be amorphous where the reaction occurs at a randomly selected depth weighted with the stopping power function and the cross section. The ejectile on his part is emitted in a direction determined by a random function regarding the angle dependent cross section. On its way it suffers hits on scattering centers and loses meanwhile energy to electrons. The ejectiles hitting onto the detectors were counted and set in relation to the same sort of ejectiles which would have reached the detector if there were no subsequent scattering. The differences in the target materials are manifested merely in the stopping power coefficients. The calculations were performed for Li, Sr and Ta. Only for high energies above 20 keV at the backward angle 130° a significant alteration can be noticed causing a slight additional anisotropy of the ^{3}He ejectiles. This can be understood from the reaction kinematics predicting an enlarged energy drop for massive ejectiles at backward angles which is further amplified by the higher energy loss and stronger scattering of the double charged ^{3}He nuclei altogether preferring the 130°-detector across from the 45° tilted target. This behaviour is a direct consequence of the concrete detector target geometry and strongly dependent on it. This also means that there is no modification at the low energies. So multiple scattering can be excluded from the possible trivial reasons for the material dependent n/p branching ratio. Moreover, the long low energy tail of the spectral lines was not obtained by the simulation which is not unexpected because of its origin from the embrittlement. Instead, the simulation disclosed that the tiny tail at the high energy side of the spectral lines, only visible with high spectral resolution, is from multiple scattering.

The embrittlement cannot be responsible for the observed anomalous asymmetry in the branching ratios, since the effects of embrittlement like tail formation rise with the projectile energy in contradiction to the deviations in the branching ratio. This is also valid for conceivable weird surface textures. Such was reconfirmed on a Ta target with an artificial blemished surface showing no differences to the usual results for Ta. Furthermore, anisotropic symmetries in crystal structures cause effects like optical activity and piezo and pyro electricity [13]. So this could be a conceivable reason for the experimental observations. Enantiomorphy is a necessary condition for such effects. However, the point groups belonging to LiD, SrD_2 and NaD do not allow for this. Transient magnetic fields can cause an alignment of the projectile nucleus relative to the interior magnetic field of ferromagnetic target materials [14,15]. Despite unfulfilled requisites, this still not fully understood phenomenon could be considered. An experiment on a ferromagnetic Fe target showed no effect.

From the theoretical point of view the cross sections for the mirror reactions ^{2}H(d, p)^{3}H and ^{2}H(d, n)^{3}He at deuteron energies below 100 keV can be described with 16 collision matrix elements, corresponding to S,P,D-waves in the entrance channel. The matrix elements for incoming D-waves cannot be omitted as frequently asserted since they are mandatory to describe the angular anisotropy down to the lowest energies. The values of the matrix elements are relatively well known and were obtained by fitting experimental cross sections, vector and tensor analyzing powers measured in gas target experiments [16, 17]. The differential cross section for both reactions can be presented by a coherent superposition of all sixteen matrix elements [8] (dashed line in fig. 5) and agrees with our results obtained for Al, Zr, Pd and Ta. In the case of Sr (also for Li) a polarization of the deuterons in the crystal lattice had to be assumed. A suppression of the channel spin $S = 0$ (spins of the deuterons are anti-parallel) and allowing

the other channels with spins $S = 1, 2$ to be undisturbed permits to describe simultaneously the enhancement of the angular anisotropy of the ^{2}H(d, n)^{3}He reaction and the decrease of the n/p branching ratio at very low energies down to 0.83. The results of corresponding calculations are presented in fig. 5 as full lines. Here we have assumed that the deuteron polarization takes place gradually below the Fermi energy (for Sr about 25 keV), reaching its maximum value already below 10 keV. A strong quenching of the neutron channel might also be explained by different screening energies for relative angular momentum $L = 0, 1$. Such was also tested and proved to be in contradiction to the experimental results. The full calculations will be subject of a forthcoming publication, also refer to [8].

4 Conclusion

We presented a first experimental evidence for an alteration of the branching ratios in the d+d fusion reactions obtained in an accelerator experiment which can be theoretically explained by polarization of the reacting deuterons in the crystal lattice. Several other conceivable but rather trivial causes could be excluded. Albeit the deeper reason for the deuteron polarization on its part is still unknown. A distinctiveness of the (earth)alkaline metals is the formation of an ionic bond to hydrogen, which might be a starting point for a possible explanation based on the spin-spin interaction mediated by electrons. The conditions in high vacuum make up for metal oxides and hydroxides in the chemical reactive targets [18] which could also be responsible for the observed effects by means of their special electron configuration and would be as such non-trivial and interesting, too.

So with the spin polarization is here another new way how the environmental electron configuration can influence immediate nuclear processes. The dense bound and free electrons in the metal can abate the Coulomb barrier in a dynamic process prior to the reaction generating a gross enhancement of the cross section which can still not be described by theory to this extent [19]. Both are dynamic processes. Static processes with respect to the electrons like alterations in the β decay of light nuclei are easier comprehensible. The screening from the electrons in the molecule CH_3T causes a shift in the spectral distribution of the β particles [20]. The removal of the two 1s electrons of ^{7}Be in the hot stellar plasma significantly increases the half-time for the decay by electron capture. Since the 1s electrons contribute by far the most to the electron density in the nucleus the modification of the orbitals of outer shell valence electrons would have only little influence on the decay parameters.

Our findings also provide a first independent support for the claim in cold fusion that requires a heavily alteration of the d+d reaction channels in contradiction to the results obtained for gas targets. Thus making it, together with the enhanced electron screening in metals [19], more credible although further efforts are necessary. An experiment with more sophisticated particle detection techniques is in progress in order to refine the data.

References

1. D.R. Tilley, H.R. Weller, G.M. Hale, Nucl. Phys. A **541**, 1 (1992).
2. Zs. Fülöp, Gy. Gyürky, E. Somorjai, D. Schürmann *et al.*, Nucl. Phys. A **758**, 697c (2005).
3. K. Czerski, A. Huke, P. Heide, M. Hoeft, G. Ruprecht, in *Nuclei in the Cosmos V*, *Proceedings of the International Symposium on Nuclear Astrophysics, Volos, Greece, July 6-11, 1998*, edited by N. Prantzos, S. Harissopulos (Editions Frontières, Paris, 1998) p. 152.
4. K. Czerski, A. Huke, A. Biller, P. Heide, M. Hoeft, G. Ruprecht, Europhys. Lett. **54**, 449 (2001).
5. F. Raiola *et al.*, Phys. Lett. B **547**, 193 (2002).
6. A. Huke, PhD Thesis, Technische Universität Berlin (2002); `http://edocs.tu-berlin.de/diss/2002/huke_armin.htm`.
7. A. Biller, K. Czerski, P. Heide, M. Hoeft, A. Huke, G. Ruprecht, in *Verhandlungen der DPG*, Vol. **1** (DPG-Frühjahrstagung, Göttingen, 1997) p. 28.
8. T. Dorsch, Diploma Thesis, Institut für Atomare Physik und Fachdidaktik der Technischen Universität Berlin (2004).
9. A. Huke, K. Czerski, T. Dorsch, P. Heide, *Proceedings of the International Conference on Condensed Matter Nuclear Science, Marseille* (2004).
10. W.M. Mueller, J.P. Blackledge, G.G. Libowitz (Editors), *Metal Hydrides* (Academic Press, New York, London, 1968).
11. R.E. Brown, N. Jarmie, Phys. Rev. C **41**, 1391 (1990).
12. A. Biller, Diploma Thesis, Institut für Atomare und Analytische Physik der Technischen Universität Berlin (1998).
13. M. Wagner, *Gruppentheoretische Methoden in der Physik* (Vieweg, Braunschweig, Wiesbaden, 1998).
14. K. Dybdal, J.S. Forster, N. Rud, Phys. Rev. Lett. **43**, 1711 (1979).
15. K.-H. Speidel, Phys. Lett. B **324**, 130 (1994).
16. H. Paetz gen. Schieck, S. Lemaitre, Ann. Phys. (Leipzig) **2**, 503 (1993).
17. O. Geiger, S. Lemaître, H. Paetz gen. Schieck, Nucl. Phys. A **586**, 140 (1995).
18. A. Huke, K. Czerski, P. Heide, Nucl. Phys. A **719**, 279c (2003).
19. K. Czerski, A. Huke, P. Heide, G. Ruprecht, Europhys. Lett. **68**, 363 (2004).
20. C.K. Hargrove, D.J. Paterson, J.S. Batkin, Phys. Rev. C **60**, 034608 (1999).